Imaging samples larger than the field of view: the SLS experience

IOP Conf. Series: Journal of Physics: Conf. Series **849** (2017) 012004 doi:10.1088/1742-6596/849/1/012004

Imaging samples larger than the field of view: the SLS experience

Ioannis Vogiatzis Oikonomidis[1,2], Goran Lovric[2,3], Tiziana P Cremona[1], Filippo Arcadu[2,4], Alessandra Patera[2,4], Johannes C Schittny[1] and Marco Stampanoni[2,4]

[1] Institute of Anatomy, University of Bern, 3012 Bern, Switzerland
[2] Swiss Light Source, Paul Scherrer Institute, 5234 Villigen, Switzerland
[3] Center for Biomedical Imaging (CIBM), EPFL, 1015 Lausanne, Switzerland
[4] Institute for Biomedical Engineering, University and ETH Zurich, 8092 Zurich, Switzerland

E-mail: ioannis.vogiatzis@ana.unibe.ch

Abstract. Volumetric datasets with micrometer spatial and sub-second temporal resolutions are nowadays routinely acquired using synchrotron X-ray tomographic microscopy (SRXTM). Although SRXTM technology allows the examination of multiple samples with short scan times, many specimens are larger than the field-of-view (FOV) provided by the detector. The extension of the FOV in the direction perpendicular to the rotation axis remains non-trivial. We present a method that can efficiently increase the FOV merging volumetric datasets obtained by region-of-interest tomographies in different 3D positions of the sample with a minimal amount of artefacts and with the ability to handle large amounts of data. The method has been successfully applied for the three-dimensional imaging of a small number of mouse lung acini of intact animals, where pixel sizes down to the micrometer range and short exposure times are required.

1. Introduction

Synchrotron X-ray tomographic microscopy (SRXTM) is an effective technique that can provide the three-dimensional (3D) structural information of samples in a non-destructive manner and with high throughput. When high spatial resolutions are employed (i.e. very small pixel sizes), the detector's field of view (FOV) is often smaller than the object's size. This is the case in respiratory studies, where the feature sizes of interest, i.e. the aleveolar septa inside the lung, are in the order of micrometers while the sample size is typically 3 orders of magnitude bigger.

A number of approaches allowing to overcome this restriction exist. Obviously, the simplest method is to combine single X-ray projection images (radiographs) that cover the whole sample and use the larger composite images to conduct the 3D reconstruction [1]. However, this leads to long acquisition times and increases computational complexity for the CT reconstruction. In addition, such an approach is very prone to misalignment artefacts in the radiography space, since they are propagated along the entire volume when reconstructing the 3D volume with the standard filtered back projection method [2]. Another approach is the so-called region of interest tomography or local tomography, where parts of the object are only partially illuminated during the entire scan [2]. The partial sinograms are then reconstructed separately and the resulting volumes are merged together. Not having the entire object within the FOV however, leads to a change in the mean value of the image and low-frequency artefacts [3].

Here we present a method to efficiently merge together different 3D volumes that have been acquired through multiple local tomographies. The overlap of the individual tomographic slices is automatically registered and then combined together through graph cuts, thus minimizing stitching artefacts.

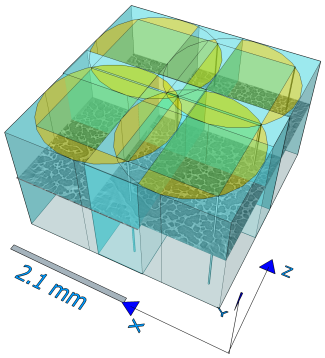

Figure 1: 2×2 spatial grid of different parts of the lung parenchyma. The areas outside of the resolution circle suffer from poor signal and contrast to noise ratio. An overlap of roughly 800 pixels was selected in order to be able to align the volumes automatically.

2. Materials and Methods

2.1. Animal Preparation, Image Acquisition and CT-reconstructions

Balb-C mice were anesthetized, placed in an upright position into a custom-made sample holder and ventilated by a small-animal ventilator (SCIREQ FlexiVent) via an endotracheal cannula. During imaging the inter-pulmonary pressure was maintained at a certain level while acquiring the tomographic scan. Animals were sacrificed by an overdose of anesthesia and images of the intact animals were taken no longer than 20 minutes afterwards. The experiments were approved and supervised by the Veterinary Service of the Cantons Aargau and Bern. Data were acquired at the X02DA TOMCAT beamline of the Swiss Light Source (SLS) at the Paul Scherrer Institute (Villigen, Switzerland). The beam was monochromatized at 21 keV by a multilayer crystal providing a good trade-off between contrast to noise ratio and resolution [4]. The in-house developed high-speed CMOS GigaFRoST detector coupled to visible-light optics of $10\times$ magnification and a 20 μm thick LuAG:Ce scintillator leading to an effective pixel size of 1.1 μm was used for the lung imaging. The tomographic scans consist of 1500 views for each volume and each projection is acquired with an exposure time of 5 ms. A single-shot propagation-based phase retrieval algorithms [5] was applied to every projection and subsequently CT-reconstructed with the *gridrec* algorithm [6] with no ring artefact removal or lens distortions corrections, since the quality of the data did not require it.

2.2. Stitching

Image stitching is performed in most cases by using invariant feature detection and matching on image pairs [7, 8]. These methods extract keypoints on the images and compute a descriptor vector for each of them. The extracted keypoints need to be detectable under changes in image scale, orientation, noise and illumination. As a result, they are usually detected on high contrast regions and near edges. The descriptor vector is then computed for every extracted feature point and normalized to unit length in order to prevent any bias due to the varying illumination.

Consequently, matching is performed between the two sets of extracted vectors, usually by means of Euclidean distance metrics. The matching is used to estimate the registration transform of the images. Outliers are detected and discarded from the set of matches in order to compute a model for the shift between the two images using least-squares fitting. The model is updated iteratively every time a new set of outliers is detected. When the probability of a correct interpolation of the images is greater than a given number, the affine transform to register the

two images has been successfully estimated. Weighted averages are performed on the basis of distance transforms, that are computed with respect to the overlapping region, and the final merged image is obtained.

In order to overcome the above problems, the following steps are here proposed to stitch the reconstructed volumes in an efficient way, while minimizing the artefacts:

(i) The tomographic scans $I_1^{m\times n\times l}$, $I_2^{m\times n\times l}$ with m, n, l the number of voxels along the 3 directions, are placed on a 2D spatial grid according to their position in real space so that the adjacent volumes can be defined. This position has not been used for the exact overlap estimation.

(ii) The two slides are registered by computing the phase correlation (PC) $R = \frac{\mathscr{F}I_1^{m\times n}\cdot\mathscr{F}I_2^{m\times n^*}}{|\mathscr{F}I_1^{m\times n}\cdot\mathscr{F}I_2^{m\times n^*}|}$ [9]. The shift is given by the position of the minimum value of the inverse Fourier transform of PC, $(\Delta x, \Delta y) = \arg\max_{(x,y)} \mathscr{F}^{-1}R$, and the same is applied on all the slices along the tomography axis, resulting in the shifted images $I_3^{o\times p\times l}$, $I_4^{o\times p\times l}$

(iii) The absolute difference image $G^{m\times n} = \left|I_3^{o\times p} - I_4^{o\times p}\right|$ of the adjacent shifted slices is computed, and the result is treated as an undirected graph with the difference values determining the cost of each node.

(iv) Two seed points v amd v' on the two opposite edges of the graph G are defined and the minimum cost path is determined as the sequence of vertices $P = (g_1, g_2, g_3, \ldots, v_{o\times p}) \in G \times G \times G \times \ldots \times G$ such that g_i is adjacent to $g_{(i+1)}$ for $1 \leq i \leq (o \times p)$ [10].

(v) The computed path is turned into a binary mask and the parts of the images I_3 and I_4 that are on each side of the path respectively are merged together, resulting in the least amount of stitching errors. The results of the masking can be seen in figure 2a - figure 2d.

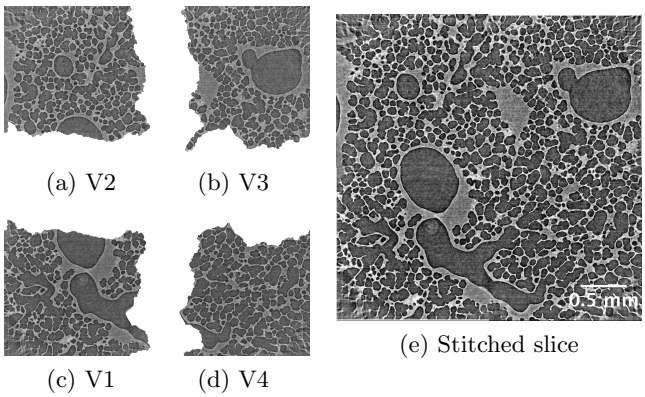

(a) V2 (b) V3 (c) V1 (d) V4 (e) Stitched slice

Figure 2: Figures (a) to (d) represent the graph cuts of the seperate volumes of the lung parenchyma, and (e) the final result of the stitching.

3. Results and Discussion

We discuss the case of a mouse lung that resulted in approximately 4500×4500 pixels shown in figure 2e. The undersampled numbered of projections per single scan (1500), is a result of the limited time window before lung collapse after death. In addition, the thickness of our scintilator and the numerical aperture of the visible light optics limit our resolution [11], thus the Nyquist tomographic sampling criterio can be relaxed. The approach is based on automatic registration of the tomographic slices of the overlap regions inside the resolution circle as depicted in figure 1. The individual slices are then combined with the use of graph cuts seen in figure 2a - figure 2d. Our approach is though general and can work on larger datasets, being limited only by the workstation memory. The method offers minimal amount of stitching artefacts, a

prerequisite when the datasets are characterized by a low contrast to noise ratio and further quantifications need to be performed. Since the validity of the final result is mostly dependent on the estimated overlap, a robust and accurate registration technique is required. Biological samples have a complex structure with no clear shape descriptor and no background because of the local tomography acquisition, making feature extraction based stitching inapplicable. In the majority of the cases the feature matching fails, since there are no clear edges between the different structures and the contrast of the image is not high enough, resulting in wrongly estimated affine registration transforms. Due to the large data size, more complex registration techniques that maximize mutual information or are based on a similar optimization approach, are also inapplicable. The fourier based registration approach provides robust and accurate results and is characetrized by computational efficiency. Furthermore, the low contrast that characterizes our datasets, makes them even more prone to the so-called *seam* artefact [12], which is produced by blending the registered overlapping images. This artefact is caused by the different illumination of the images and results in a visible border separating the original input images. The only way to mitigate it, within the context of a blending approach, is with more sophisticated weighting approaches that, compromising however the resolution. By employing a graph cut approach, the images are stitched together like different pieces of a puzzle. Thus, we completely avoid any kind of blending and along with it the *seam* artefact.

4. Conclusion

In this work we have presented a methodology for increasing the FOV of SXRTM. Neighbouring reconstructed volumes are stitched together to increase the FOV by means of an effective graph-cuts based algorithm. The *seam* artefact, present in weighted blending merged datasets, is suppressed without compromising the local resolution. Complex weighting averages approaches that are used to suppress seam artefacts are computationally expensive and make the stitching procedure slower as the slice size increases. With the proposed method single slices are combined together like a puzzle without having to recompute weighted blending every time an adjacent slice is to be merged with the rest and thus altering the contrast of the initial datasets.

Acknowledgments

We would like to acknowledge Dr. Christian M Schlepütz for his support at the TOMCAT beamline and for carefully reading the manuscript. We are thankful for the grants 310030-153468 and CR23I2-135550 of the Swiss National Science Foundation.

References

[1] Haberthür D, Hintermüller C, Marone F, Schittny J C and Stampanoni M 2010 *Journal of synchrotron radiation* **17** 590–599
[2] Kyrieleis A, Titarenko V, Ibison M, Connolley T and Withers P 2011 *Journal of microscopy* **241** 69–82
[3] Rashed E A and Kudo H 2013 *Journal of synchrotron radiation* **20** 116–24
[4] Lovric G, Barré S F, Schittny J C, Roth-Kleiner M, Stampanoni M and Mokso R 2013 *Journal of applied crystallography* **46** 856–860
[5] Moosmann J, Hofmann R and Baumbach T 2011 *Optics express* **19** 12066–73
[6] Marone F and Stampanoni M 2012 *Journal of synchrotron radiation* **19** 1029–37
[7] Lowe D G 1999 *Computer vision, 1999. The proceedings of the seventh IEEE international conference on* vol 2 (Ieee) pp 1150–57
[8] Brown M and Lowe D G 2007 *International journal of computer vision* **74** 59–73
[9] Guizar-Sicairos M, Thurman S T and Fienup J R 2008 *Optics letters* **33** 156–58
[10] Dijkstra E W 1959 *Numerische mathematik* **1** 269–71
[11] Stampanoni M, Borchert G, Wyss P, Abela R, Patterson B, Hunt S, Vermeulen D and Rüegsegger P 2002 *Nuclear Instruments and Methods in Physics Research Section A: Accelerators, Spectrometers, Detectors and Associated Equipment* **491** 291–301
[12] Levin A, Zomet A, Peleg S and Weiss Y 2004 *European Conference on Computer Vision* (Springer) pp 377–89